JOURNAL OF APPLIED POLYMER SCIENCE VOL. 18, PP. 1869–1889 (1974)

A Relationship Between the Fracture Mechanics and Surface Energetics Failure Criteria

D. H. KAELBLE, *Science Center, Rockwell International, Thousand Oaks, California 91360*

Synopsis

The reversible part of the fracture mechanics (F-M) fracture energy γ_c is redefined in terms of current theory for surface energetics (S-E) interactions at regular interfaces. These new failure criteria are applied to the definition of surface energy criteria for spontaneous interfacial failure, where $\gamma_c = 0$, produced by selected conditions of liquid-phase immersion. For cases where $\gamma_c > 0$, the total fracture energy $W = \gamma_c + W_p$, where the irreversible plastic work of surface formation $W_p \approx W \gg \gamma_c$. A qualitative relation between $\gamma_c^{1/2} \propto W_p$ is observed for the case of steady-state crack propagation in peeling. For adsorption bonds, the theory provides a new method of mapping the surface energy effects of the immersion phase upon the Griffith fracture energy γ_c. Essential factors which determine water sensitivity of interfacial bonds are incorporated into the analysis and experimentally verified.

INTRODUCTION

Theories of adhesion and cohesion have progressed along several divergent avenues, which are: (a) theories of bond strength based upon the fracture mechanics (F-M) criterion of critical flaw size[1–4] and (b) the surface energetics (S-E) theories of molecular forces at interfaces.[5,6] The F-M theory applies principles of continuum mechanics and stress analysis, while the S-E theory operates at the atomistic or molecular level of response. The operational advantages of the continuum visualization are obvious and well documented in defining parameters for engineering design. The difficulty with this approach is that the physical chemistry of fracture is left largely undefined.

The S-E theory has recently been extended to treat vapor/liquid/solid, liquid/liquid/solid, and solid/liquid/solid interactions.[6] The objective of this discussion is to introduce these new relations into the F-M model for crack propagation. Of particular interest is the examination of the effects of varied vapor- or liquid-phase immersion conditions upon the F-M criterion for adhesive and cohesive joint strength.

THEORY

The Griffith model for failure by crack propagation is based on the following assumptions[1,2]: (1) The crack is an ellipse of vanishing minor axis.

(2) Hooke's law applies up to the corners of the crack. (3) The plane of the crack is perpendicular to the applied load. (4) The crack will grow spontaneously when the rate of decrease in stored elastic energy within the material equals or exceeds the rate of surface energy increase. The first three assumptions define a two-dimensional case of a flat plate with an elliptical crack extending through its thickness. The stress analysis for this case, due to Inglis,[7] provides the following relation for stress concentration at the crack tip:

$$\frac{\sigma_0}{\sigma} = 1 + 2\left(\frac{c}{r}\right)^{1/2} \simeq 2\left(\frac{c}{r}\right)^{1/2} \tag{1}$$

where σ_0 = maximum stress at the crack tip, σ = applied stress on the plate normal to the plane of the crack, c = depth of a surface crack or one half the length for an ellipse cut through the interior of the sheet, and r = radius of curvature at the crack tip.

The fourth of the above assumptions provides the following familiar Griffith relation for the case of plane stress:

$$\sigma \leq \sigma_c = \left(\frac{2E\gamma_c}{\pi c}\right)^{1/2} \tag{2}$$

where σ_c = critical value for the applied stress σ acting on the plate normal to the plane of the crack, E = Young's modulus of the plate material, and γ_c = surface (or interfacial) energy of the crack surface. Equation (2) provides a simple mathematical model which correlates material strength (σ_c) to a rheological property (E), a surface property (γ_c), and a microgeometry (c). In brittle materials where eq. (2) is meant to apply, the natural cracks which determine strength have small dimensions, $c \leq 1$ μm, with $2r$ approaching molecular dimensions.

For materials which display slight ductility so that plastic flow occurs at the crack tip during crack propagation, it is known that eq. (1) no longer applies, and other approximations are required to define the stress field at the crack tip. Orowan[8] suggested the following modification for the Griffith failure criteria:

$$\sigma \leq \sigma_c = \left[\frac{2E(\gamma_c + W_p)}{\pi c}\right]^{1/2} \approx \left[\frac{2EW_p}{\pi c}\right]^{1/2} \tag{3}$$

where W_p = work of plastic deformation per unit of surface formation. Organic and polymeric solids display solid surface tensions γ which range from 9 to 50 dyn/cm, as deduced from wettability measurements.[9] Inorganic and metallic surfaces, in the absence of organic contamination, are estimated to display surface tensions γ ranging from 500 to 5000 dyn/cm. Measured values of $\gamma_c + W_p$ from fracture mechanics experiments provide the typical values reported in Table I. These data point out that W_p may be a minor factor in the fracture of glass which behaves as a brittle solid. With tough solids such as PMMA and steel, the surface tension contribu-

TABLE I
Typical Experimental Values for Total Energy of Surface Formation ($\gamma + W_p$) from Fracture Mechanics Studies[a]

Material	Experimental ($\gamma + W_p$), dyn/cm
Glass	550
Poly(methyl methacrylate) (PMMA)	3×10^5
Steel	1×10^6

[a] From Berry and Bueche.[10]

tion γ_c may become a negligible part of $\gamma_c + W_p$, and the major resistance to crack propagation appears due to W_p.

Irwin has extended the Griffith theory to treat the case of elastic-plastic materials by a method which retains the linear-elastic assumptions and provides the Griffith equation as a limiting case. The relations derived by Irwin for plane stress are as follows[3,4]:

$$\sigma \leq \sigma_c = \left(\frac{E\mathcal{G}_{1c}}{\pi c}\right)^{1/2} = \frac{K_{1c}}{\alpha(\pi c)^{1/2}} \tag{4}$$

$$K_1 = \alpha\sigma(\pi c)^{1/2} = (E\mathcal{G}_1)^{1/2} \tag{5}$$

$$K_{1c} \approx [2E(\gamma_c + W_p)]^{1/2} \tag{6}$$

where $\mathcal{G}_{1c}$ = the critical strain energy release rate for fast crack propagation, K_{1c} = the critical stress intensity factor, and α is a geometrical correction factor ($\alpha = 1.0$ for a central crack in a thin infinite plate). Equation (5) expresses the equivalence between stress intensity K_1 and energy release rate $\mathcal{G}_1$ approaches, while eq. (6) expresses the correlation between critical stress intensity K_{1c} and the Griffith-Orowan terms. The Irwin analysis has been applied to a number of adhesive joint systems where both adhesive and cohesive fracture modes are recognized in the double cantilever beam (DCB) geometry of loading.[11-17] Williams and co-workers[18-22] have extensively applied the Griffith-Orowan criteria to the study of both adhesive and cohesive failure where crack propagation by pressurizing a blister according to the method of Dannenberg.[23]

Starting with the pioneering studies of Zisman and co-workers,[9] a number of refinements have been introduced in the description of solid surface tension and the analytical definitions of interfacial tension and works of adhesion. Important theoretical contributions due to Fowkes[24] and Good[25] have recently been applied by a number of workers.[26-30] Although the detailed form of the relations for surface and interfacial free energy varies, the central notion is expressed in the following relation[5,6]:

$$\gamma_{ij} = (\alpha_i - \alpha_j)^2 + (\beta_i - \beta_j)^2 + \Delta_{ij} \tag{7}$$

where γ_{ij} = the interfacial tension at the interface between phase i and phase j; α_i, α_j = the half-powers of the dispersion (London) part of the surface tensions; β_i, β_j = the half-powers of the polar (Keesom) part of the surface tensions; and Δ_{ij} = an excess term due to ionic or covalent inter-

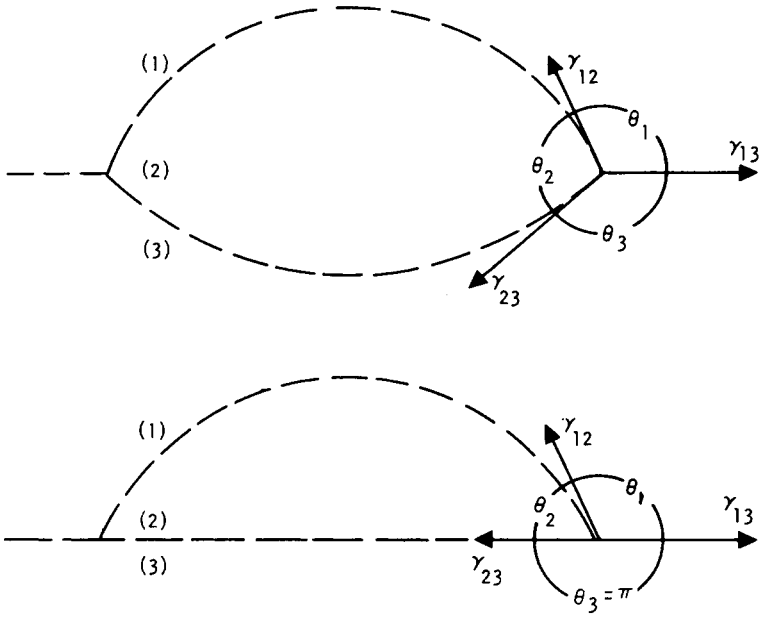

Fig. 1. Illustrative schematic of the influence of solid state constraints, where $\theta_3 = \pi$, upon the equilibrium contact angles between phases (1), (2), and (3).

actions. Interfaces dominated by van der Waals interactions are termed regular interfaces, and the value of the excess term Δ_{ij} may be considered negligible. Ideal interfaces are described in eq. (7) by the case where $\gamma_{ij} = 0$. The liquid–vapor or solid–vapor surface tensions are automatically defined from eq. (7) by the following relations:

$$\gamma_{iv} = \alpha_i^2 + \beta_i^2 = \gamma_{iv}^d + \gamma_{iv}^p \tag{8}$$

$$\gamma_{jv} = \alpha_j^2 + \beta_j^2 = \gamma_{jv}^d + \gamma_{jv}^p. \tag{9}$$

Setting $\alpha_j = \beta_j = 0$ in eq. (7) (phase j = vapor state) provides eq. (8). The converse statement, $\alpha_i = \beta_i = 0$, for vapor phase i provides eq. (9). In a three-phase system where interdiffusion (co-solubility) restraints limit interfacial interactions to adsorption mechanisms, it is evident that the spreading coefficients S_1, S_2, and S_3 provide the most general criteria for describing spontaneous mechanisms of bonding and debonding.[5,6] These spreading coefficients, for phases 1, 2, and 3, respectively, are described by balances of interfacial tension as follows:

$$S_1 = \gamma_{23} - \gamma_{12} - \gamma_{13} \tag{10}$$

$$S_2 = \gamma_{13} - \gamma_{23} - \gamma_{12} \tag{11}$$

$$S_3 = \gamma_{12} - \gamma_{13} - \gamma_{23} \tag{12}$$

where γ_{12}, γ_{13}, and γ_{23} = interfacial tensions at the 1–2, 1–3, and 2–3 interfaces, respectively. A correlation between the interfacial tensions described by the above relations and the contact angles θ_1, θ_2 and θ_3 formed between phases is shown by the schematic of Figure 1. The upper view of Figure 1

illustrates the equilibrium obtained in the absence of gravitational effects and solid-state constraints. The lower view illustrates the case where $\theta_3 = \pi$ rad $= 180°$ due to solid state constraints on phase 3. It follows that, when $S_i \geqslant 0$ for any one of the mobile phases $i = 1, 2, 3$ in the illustration of Figure 1, the contact angle $\theta_i = 0$, and that phase will spontaneously extend its surface area to separate the two remaining phases.

The basic relations for both the F-M and the S-E theories have been redeveloped in the above discussion so that the propositions involved in their combination are clearly understood. The objective of the following discussion is to provide a more detailed connection between the interfacial tension balances depicted in Figure 1 and the mechanics criteria for crack propagation shown schematically by Figure 2. The left view of Figure 2 depicts two solid phases (1) and (3) joined by a solid interface indicated by the line that extends ahead of the edge crack of length c and end radius r. Phase (2) has access to the crack surface; and under some critical plane stress $\sigma = \sigma_c$, fracture occurs. The right-hand view of Figure 2 depicts the separated parts with the extension of phase (2) to fill the region originally involved in interfacial bonding. Since Figure 2 indicates the stress acting in series across phase (1) and phase (3), it is appropriate to define a composite plate modulus E as follows[5]:

$$E = \frac{E_1 E_3}{\phi_1 E_3 + \phi_3 E_1} \tag{13}$$

where the fractional lengths are defined as

$$\phi_1 = 1 - \phi_3 = L_1/(L_1 + L_3). \tag{14}$$

By substituting Young's modulus defined by eq. (13) into eq. (2) through eq. (6), the proposition that strain energy is stored dominantly in the more compliant phase is properly taken into account. Thus, if $\phi_1 = \phi_3$ and $E_3 >>> E_1$, we obtain $E \approx (E_1/\phi_1)$ in the crack propagation criteria. This is by no means a trivial consideration for the interface between a metal (phase 3) where $E_3 \geqslant 7.0 \times 10^{11}$ dyn/cm^2 and a polymer (phase 1) where for the glass state $E_1 \simeq 3.5 \times 10^{10}$ dyn/cm^2 and for the rubbery state, $E_1 \simeq 3.5 \times 10^6$ dyn/cm^2. In these cases, the energy release defined by eq. (5) or eq. (6) is dominantly contributed by the more compliant polymer phase.

The second modification of the F-M relations is obtained by defining the Griffith surface energy γ_c in explicit terms of reversible free energy change due to crack extension. This correlation interconnects the illustrations of Figure 1 and Figure 2 by the relation

$$2\gamma_c = \left(\frac{\partial F_2}{\partial \Gamma_2}\right)_{v,T} = -S_2 \tag{15}$$

where F_2 = the surface free energy of phase 2, Γ_2 = the total surface area of phase 2, and γ_c and S_2 are defined, respectively, by eqs. (2) and (11). As a crack extends to debond a unit area of interface, two unit areas of new surface are created, thus accounting for the factor $2\gamma_c$ in eq. (15). The

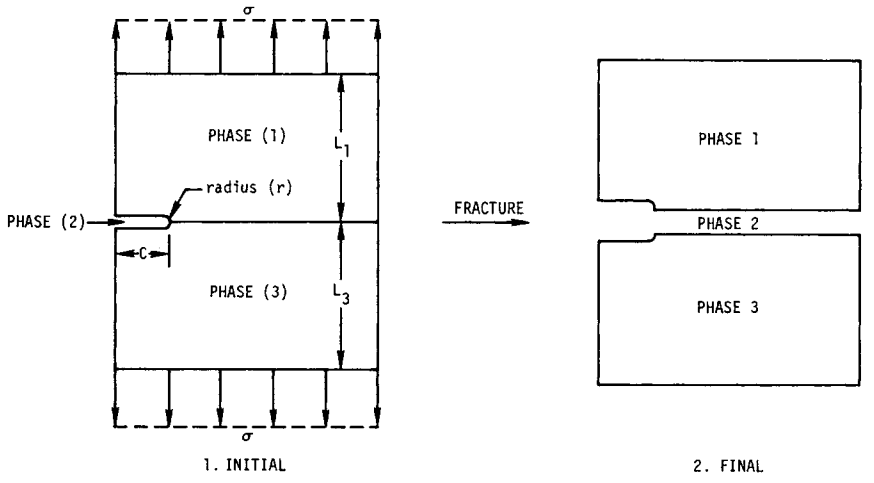

Fig. 2. Interface failure under plane stress.

definition of phase 2 surface area Γ_2 in eq. (15) automatically accounts for this proposition, thus making $2\gamma_c = -S_2$.

For regular adsorption interfaces, where $\Delta_{ij} = 0$ in Eq. (7), we can substitute this expression for i–j = 1–2, 1–3, and 2–3 into eq. (11) to obtain the following detailed expression for S_2 as follows[6]:

$$S_2 = 2[\alpha_1\alpha_3 + \beta_1\beta_3 + \alpha_2\alpha_3 + \beta_2\beta_3 - \alpha_1\alpha_2 - \beta_1\beta_2 - \gamma_{2v}].$$

Substituting the above expression into eq. (15) defines the Griffith surface energy term as follows:

$$\gamma_c = [\alpha_1\alpha_3 + \beta_1\beta_3 + \gamma_{2v} - \alpha_2\alpha_2 - \beta_1\beta_2 - \alpha_2\alpha_3 - \beta_2\beta_3]. \tag{16}$$

Equation (16) is a general expression that must reduce to provide all the expected specific relations for works of adhesion or cohesion as special cases. The first demonstration involves the case where phase 2 is the vapor phase with $\gamma_{2v} = \alpha_2 = \beta_2 = 0$. By substitution of these zero values into eq. (16) we obtain

$$\gamma_c = \alpha_1\alpha_3 + \beta_1\beta_3 = \frac{W_{13}}{2} \tag{16a}$$

which states that γ_c is one half the interfacial work of adhesion between phase 1 and phase 3 under vapor immersion. For the further special case of vapor immersion $\gamma_{2v} = \alpha_2 = \beta_2 = 0$ and an ideal interfacial bond where $\alpha_1 = \alpha_3$ and $\beta_1 = \beta_3$, we obtain from eq. (16) the following relation:

$$\gamma_c = \gamma_{1v} = \gamma_{3v} = W_c/2 \tag{16b}$$

where γ_{1v} and γ_{3v} are the respective surface tensions of phases 1 and 3 and W_c is the reversible work of cohesion of either phase. It is evident that eq. (15), or its more specific expression in eq. (16), provides the standard defini-

tions of the thermodynamic criteria of surface formation. The important new feature of eq. (16) is, of course, the added capability to describe the effects of the immersion phase upon γ_c in terms of α_2, β_2, and $\gamma_{2v} = \alpha_2^2 + \beta_2^2$.

In order to conveniently visualize and utilize this interdependency of γ_c upon α_2 and β_2, we may rewrite eq. (16) in the following form:

$$\gamma_c = -\frac{S_2}{2} = \alpha_2^2 + \beta_2^2 - (\alpha_1 + \alpha_3)\alpha_2 - (\beta_1 + \beta_3)\beta_2 + \alpha_1\alpha_3 + \beta_1\beta_3. \quad (17)$$

Equation (17) is recognizable as a circular parabola in γ_c, α_2, β_2 Cartesian space as defined by the following coefficients:

$$\gamma_c = -\frac{S_2}{2} = R^2 - R_0^2 \quad (18)$$

where

$$R_0^2 = \frac{1}{4}[(\alpha_1 - \alpha_3)^2 + (\beta_1 - \beta_3)^2]$$

$$R^2 = (\alpha_2 - H)^2 + (\beta_2 - K)^2$$

$$H = \frac{1}{2}(\alpha_1 + \alpha_3)$$

$$K = \frac{1}{2}(\beta_1 + \beta_3).$$

By substituting eqs. (13) and (18) into the Griffith eq. (2), we obtain the new failure criteria

$$\sigma_c = \left[\frac{E_1E_3}{\phi_1E_3 + \phi_3E_1}\frac{2(R^2 - R_0^2)}{\pi c}\right]^{1/2} \geqslant 0 \quad (19)$$

for the idealized case of brittle crack propagation where the Orowan plastic work term $W_p = 0$. Equation (19) is presented as an expression which incorporates more detailed information for the special case described by Figure 2 than the original Griffith criteria of eq. (2). For eq. (19) to operate in a strict physical sense, the original assumptions of the Griffith theory must still apply, and therefore no consideration is included of crack extension rate effects or plastic work at the crack tip. Inspection of eqs. (5) and (6) shows that in the limit where $K_{1c} = (2E\gamma_c)^{1/2}$, the Griffith, Orowan, and Irwin failure criteria converge and become identical to each other.

One of the dramatic new features of eq. (19) is the implicit prediction that an immersion phase that provides $R \leqslant R_0$ should reduce σ_c to $\sigma_c = 0$ and cause failure in the absence of external load, as described in Figure 2 when $\sigma_c = 0$. In this instance, the origin of plastic work W_p due to conversion of elastically stored strain energy of external loading is eliminated, since $\sigma = 0$ and the Griffith and Irwin criteria are identical. Figure 3

provides a schematic visualization of the case where the condition $R \leqslant R^0$ or $S_2 \geqslant 0$ provides a contact angle $\theta_2 = 0$ which permits the formation of a new Griffith crack of molecular dimensions at the interface between phase 1 and phase 3. The radius of curvature r_2 is just one half the diameter d_2 of the intruding phase 2 molecules. The interfacial stress supplied by this intermolecular Griffith crack, with semiinfinite length to radius $c/r_2 \rightarrow \infty$ is roughly described by the relation

$$\sigma_2 \left(\frac{\text{dyn}}{\text{cm}^2}\right) \approx \frac{S_2}{d_2} = \frac{\gamma_{13} - \gamma_{23} - \gamma_{12}}{2r_2} \geqslant 0. \tag{20}$$

Assume, for example, that $S_2 = 1.0$ dyn/cm and $r_2 = (2 \text{ to } 10) \times 10^{-8}$ cm, one obtains appreciable values of $\sigma_2 = (1.0 \text{ to } 5.0) \times 10^7$ dyn/cm^2 (142 to 710 psi) as a significant interfacial stress which promotes spontaneous failure.

The above relations are now applied to the analysis of published data that describe cases of purely thermodynamic failure where the applied stress $\sigma = 0$ and kinetic failure where $\sigma \geqslant 0$ and is influenced by the magnitude of γ_c as defined by eq. (18).

Thermodynamic Failure ($\sigma = 0$)

Owens has recently reported instances of spontaneous failure of polymer–polymer interfaces by immersion in aqueous detergent solutions in the absence of applied external load.[31] The analysis applied by Owens is formally equivalent to the statements provided by eq. (7) through eq. (12) of this discussion, except that Owens describes surface tension $\gamma_{iv} = \gamma_{iv}^d + \gamma_{iv}^h$ in terms of additive dispersion and hydrogen bonding parts. By specifying that

$$\gamma_{iv}^h = \gamma_{iv}^p = \beta_i^2$$

the results of this interesting study can be analyzed in terms of the theory developed here. Owens prepared laminates of flamed polypropylene (phase 1) which were coated with a thin layer of a poly(vinylidene chloride) copolymer (phase 3). Analysis of Owen's data shows that, for phase 1, $\alpha_1 = 5.79$, $\beta_1 = 2.03$ (dyn/cm)$^{1/2}$, while for phase 3, $\alpha_3 = 6.24$, $\beta_3 = 3.84$ (dyn/cm)$^{1/2}$. Inserting these surface properties into eq. (18) defines the constants $H = 6.02$, $K = 2.93$, $R_0 = 0.93$ (dyn/cm)$^{1/2}$ for the 1–3 interface formed by these interacting solids. The surface tension properties of the aqueous detergent solutions characterized by Owens are summarized in terms of α_2 and β_2 in Table II. The position of these phase 2 surface properties are located on the surface energy diagram of Figure 4, which has coordinates of α_2 versus β_2.

Figure 4 is a new form of graphic presentation by which the surface properties of a liquid or vapor immersion phase 2 can be directly correlated. The anticipated zone of spontaneous interfacial failure, defined through eq. (18) in terms of H, K, and R_0, is shown in Figure 4 as the circular region wherein $S_2 \geqslant 0$. When the surface tension properties of phase 2 fall within

TABLE II
Surface Properties of Aqueous Detergent Solutions
Above the Critical Micelle Concentration[a]

No.	Immersion phase 2	γ_{2V}	α_2	β_2	Conc., %
1	Water	72.8	4.67	7.14	0
2	Sodium diisobutylsulfosuccinate	43.3	4.07	5.17	1.0
3	Sodium *n*-octylsulfate	41.4	5.16	3.85	3.5
4	Triton X-405[b]	42.4	5.42	3.61	1.0
5	Sodium *n*-decylsulfate	39.5	5.29	3.39	1.0
6	Sodium *n*-tetradecylsulfate	36.7	5.30	2.93	0.2
7	Sodium *n*-dodecylsulfate	37.2	5.39	2.86	0.5
8	Sodium *n*-hexadecylsulfate	36.0	5.29	2.68	0.05
9	Sodium diisoamylsulfosuccinate	25.6	4.87	1.38	1.0
10	Sodium di(2-ethylhexyl)sulfosuccinate	25.8	4.96	1.05	1.0
11	Dry air	0.0	0.0	0.0	

[a] From Owens.[31]

[b] Octylphenol–ethylene oxide condensate.

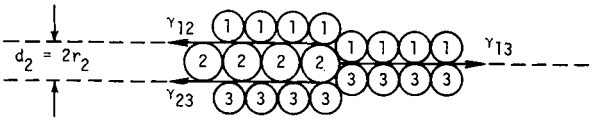

Fig. 3. Schematic of the intrusion of phase (2) molecules at the phase (1)–phase (3) interface when the spreading coefficient $S_2 = \gamma_{13} - \gamma_{12} - \gamma_{23} \geqslant 0$.

the $S_2 \geqslant 0$ region, spontaneous debonding is predicted. Experiments of Owens showed that detergent solutions no. 4–8 did produce spontaneous interfacial failure of the phase 1–phase 3 bond in a failure time $t_b \leqslant 15$ min under no external stress, $\sigma = 0$. Conversely, immersion for over six months in water and detergent solutions no. 2, 3, 9, and 10 produced no spontaneous failure.

An analysis of Owens' data in the terms provided by eqs. (18) and (19) is summarized in Table III. The resulting curves of the square root of the Griffith surface energy $\gamma_c^{1/2} \propto \sigma_c$ and the spreading coefficient S_2 are plotted against the radius R in Figure 5. It may be noted in eq. (18) that positive values of S_2 produce negative values of γ_c. Since the Griffith equation correlates $\sigma_c \propto \gamma_c^{1/2}$, it follows that negative values of γ_c correlate with nonphysical (imaginary) values of $(-1)^{1/2}\gamma_c^{1/2}$. In Table III, these values are listed in parenthesis and it is assumed $\gamma_c = 0$ for these cases. The curves of Figure 5 now include all the phase 2 points from Figure 4 on a single function of $\gamma_c^{1/2}$ versus R. This illustration shows that the function of S_2 versus R, a parabola with a maximum value of $S_2 = 1.74$ dyn/cm at $R = 0$ and a minimum value of $S_2 = -88.04$ dyn/cm at $R = 6.70$ (dyn/cm)$^{1/2}$, characterizes the air immersion condition. Contrasting to the smooth variation of S_2 with R we note that the function of $\gamma_c^{1/2}$ versus R maintains values of $\gamma_c^{1/2} = 0$ where $R < R_0$ and then rises abruptly

TABLE III
Analysis for Criteria of Spontaneous Failure Under Phase 2 Immersion for an Interfacial Bond with Coefficients $H = 6.02(\text{dyn/cm})^{1/2}$, $K = 2.93(\text{dyn/cm})^{1/2}$, and $R_0 = 0.93(\text{dyn/cm})^{1/2}$

Immersion phase 2 (from Table II)	R, $(\text{dyn/cm})^{1/2}$	S_2, dyn/cm	$\gamma_c^{1/2}$, $(\text{dyn/cm})^{1/2}$ [a]
1	4.30	−35.3	4.20
2	2.97	−15.9	2.82
3	1.26	−1.44	0.85
4	.91	.10	0.0 (0.25i)
5	.86	.26	0.0 (0.36i)
6	.72	.70	0.0 (0.59i)
7	.64	.92	0.0 (0.68i)
8	.76	.58	0.0 (0.54i)
9	1.93	−5.70	1.69
10	2.16	−7.58	1.94
11	6.70	−88.04	6.64
$\alpha_2 = H$, $\beta_2 = K$	0.0	1.74	0.0 (0.93i)

[a] $i = (-1)^{1/2}$.

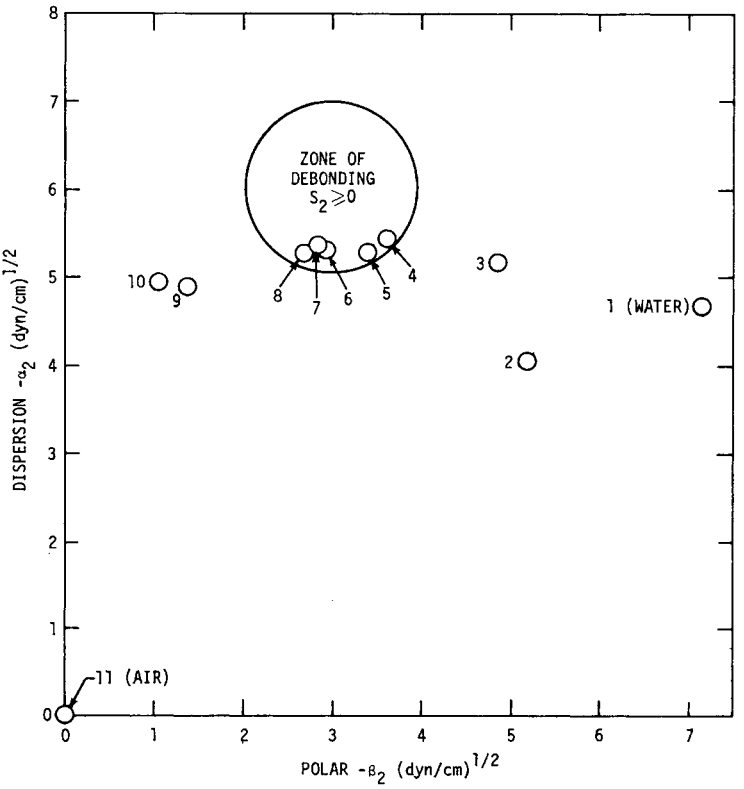

Fig. 4. Calculated zone of spontaneous debonding, where $S_2 \geq 0$, for a phase (1)–phase (3) interface relative to the α_2,β_2 surface properties of the immersion phase (2).

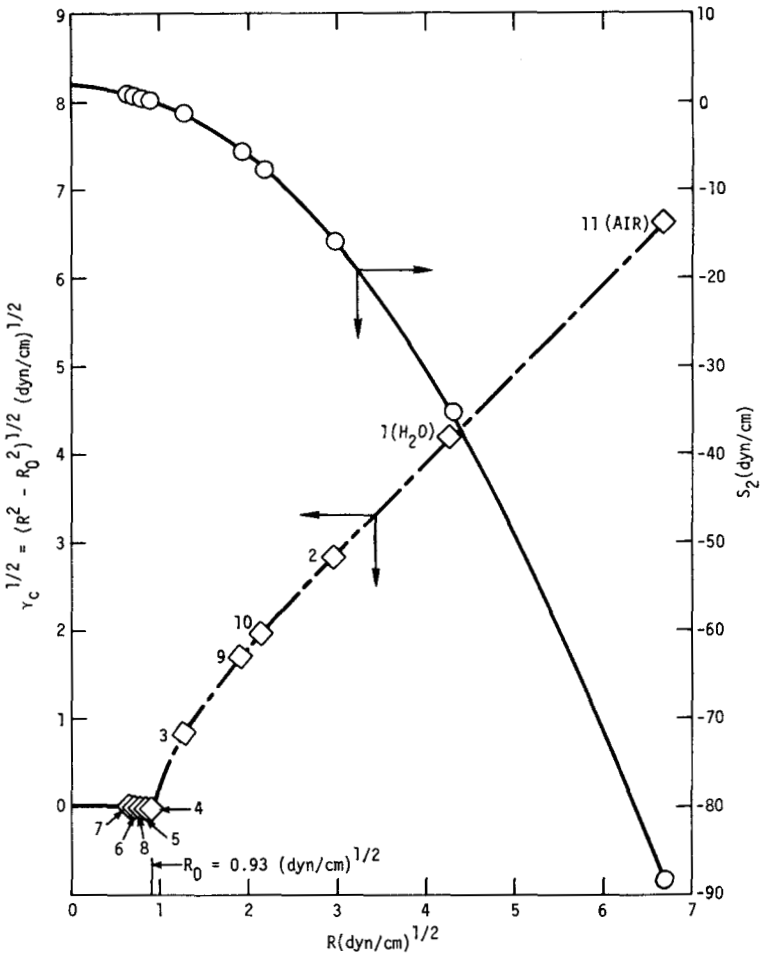

Fig. 5. Calculated functions of S_2 and $\gamma_c^{1/2}$, relative to the locus H, K of the zone of debonding.

when $R > R_0$. This abrupt discontinuity in the $\gamma_c^{1/2}$ function at R_0 appears to correlate with the dramatic change in the time scales of $t_b \leqslant 15$ min when $S_2 \geqslant 0$ to $t_b \geqslant 6$ months when $S_2 \leqslant 0$ reported by Owens. This analysis and the curves of Figure 5 appear to provide a clarification of the reasons why small but positive values of $0 \leqslant S_2 \leqslant 2.8$ dyn/cm operate in dramatic fashion to produce spontaeous rupture. While the $\gamma_c^{1/2}$-versus-R curve of Figure 5 predicts that water and other detergent solutions with $R > R_0$ should reduce bond strength without producing spontaneous failure, no test of this prediction is available in the study conducted by Owen. More recent experiments, reported by Gent and Schultz,[32] provide data which lie in the range $R > R_0$ where external force is required to propagate a crack. Analysis of these data provide a further test of the modified

equation under nonthermodynamic conditions where the applied stress $\sigma > 0$.

Nonthermodynamic Failure ($\sigma = 0$)

When two flexible but inextensible materials are delaminated in the T-peel geometry described in Figure 6, the fracture energy is described by the following relation:

$$W = P/b \approx \gamma_c + W_p \tag{21}$$

where W = total cleavage work per unit area of fracture surface, P = peeling force, and b = bond width. Equation (21) subdivides this total work W into a reversible part γ_c and an irreversible part W_p, as suggested by Orowan. The study of Gent and Schultz[32] concerns the effects of liquid immersion upon the function of peeling work W versus peeling rate $\dot{c} = dc/dt$. This study represents a case where liquid immersion failed to produce spontaneous failure, since $\gamma_c \geqslant 0$, but did substantially influence the cleavage work W. The system examined in the study of Gent and Schultz involves a laminate of a crosslinked elastomer (60/40 butadiene/styrene copolymer) containing a cotton cloth reinforcement as phase 1 bonded to a polyester [poly(ethylene terepthalate)] film as phase 3. Both phase 1 and phase 3 surfaces were characterized by contact angle measurements with reference pure liquids and ethanol–water mixtures. A summation of these

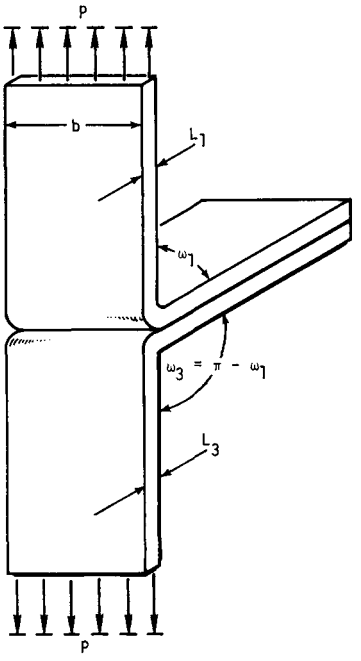

Fig. 6. Schematic illustration of the T-peel test geometry.

TABLE IV
Analysis of α_1 and β_1 for Elastomer and α_3 and β_3 for Polyester Surfaces[a]

	γ_{Lv} (dyn/cm)	$2\alpha_L$ $(\text{dyn/cm})^{1/2}$	β_L/α_L	Elastomer $W_{21}/2\alpha_L$ $(\text{dyn/cm})^{1/2}$	Polyester $W_{L3}/2\alpha_L$ $(\text{dyn/cm})^{1/2}$
Pure Liquid					
Water	72.8	9.34	1.54	6.26	9.35
Glycerol	63.4	11.66	0.94	6.21	8.14
Formamide	58.2	11.37	0.90	6.64	7.97
Diiodomethane	50.8	13.90	0.22	6.07	6.94
Ethylene glycol	47.7	10.83	0.81	5.90	7.15
Ethanol	22.7	8.24	0.56	5.34	$\theta_L = 0$
Ethanol–Water Mixtures (vol-% H_2O)					
100	72.8	9.34	1.54	6.26	9.35
90	51.3	8.92	1.26	5.76	8.35
80	41.5	8.84	1.06	5.15	7.33
70	36.0	8.32	1.04	5.20	7.40
50	30.0	8.76	0.75	4.70	6.66
30	27.2	8.80	0.64	4.95	$\theta_L = 0$
10	24.0	8.44	0.59	5.05	$\theta_L = 0$
0	22.7	8.24	0.56	5.34	$\theta_L = 0$

Solid Surface Properties: Units of $\alpha,\beta = (\text{dyn/cm})^{1/2}$

(1) Pure liquid interactions:

Elastomer	$\alpha_1 = 6.04$	$\beta_1 = 0.14$
Polyester	$\alpha_3 = 6.54$	$\beta_3 = 1.83$

(2) Ethanol/water mixtures:

Elastomer	$\alpha_1 = 3.10$	$\beta_1 = 2.05$
Polyester	$\alpha_3 = 3.75$	$\beta_3 = 3.64$

[a] γ_{Lv} and W_{L1} and W_{L3} Data from Gent and Schultz[32]; α_L data from Fowkes[24] and Dann.[33]

data, organized into a format for isolation of α_1 and β_1 for the elastomer and α_3 and β_3 for the polyester surfaces, is presented in Table IV. The Young equation $W_{L1} = \gamma_{Lv}(1 + \cos\theta_{L1})$ is applied to convert the contact angle θ_{L1} data reported by Gent and Schultz to interfacial work of adhesion W_{L1}. The adsorption theory provides the following analyical expression[6]:

$$\frac{W_{L1}}{2\alpha_L} = \alpha_1 + \beta_1\left(\frac{\beta_L}{\alpha_L}\right). \tag{22}$$

Equation (22) provides for isolation of α_1 as an intercept and β_1 as a slope of a linear curve of $W_{L1}/2\alpha_1$ versus β_L/α_L for elastomer phase 1. In similar fashion, the contact angle θ_{L3} data on the polyester phase 3 were converted to interfacial works of adhesion $W_{L3} = \gamma_{Lv}(1 + \cos\theta_{L3})$ and analyzed by the following expression:

$$\frac{W_{L3}}{2\alpha_L} = \alpha_3 + \beta_3\left(\frac{\beta_L}{\alpha_L}\right). \tag{23}$$

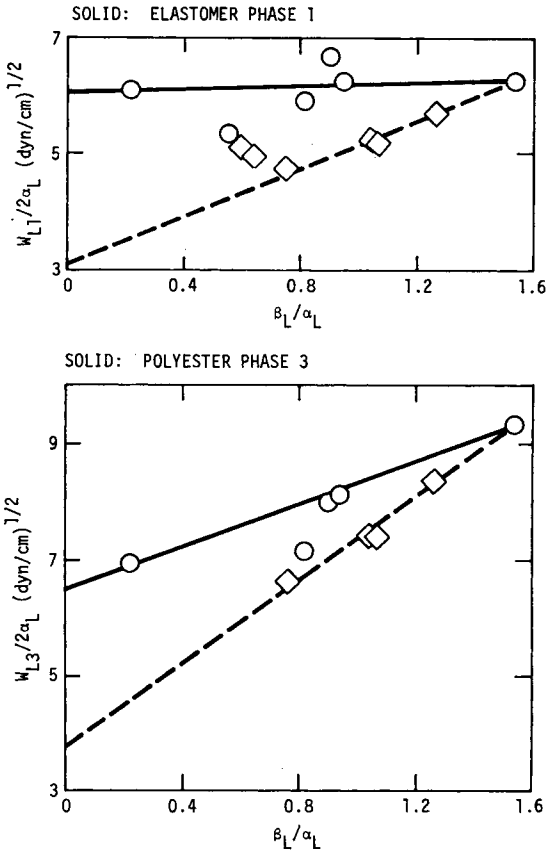

Fig. 7. Graphic definition of solid surface tension coefficients α_1,β_1 for phase (1) and α_3,β_3 for phase (3).

The values of α_L and β_L presented in Table IV are based upon the determinations of $\gamma_{Lv}{}^d$ and $\gamma_{Lv}{}^p = \gamma_{Lv} - \gamma_{Lv}{}^d$ determined in studies by Fowkes[24] and Dann.[33]

The data of Table IV, plotted according to the format defined by eq. (22) and eq (23), are shown in the illustrations of Figure 7. One notes that the $W_{L1}/2\alpha_L$ and $W_{L3}/2\alpha_L$ values for the ethanol–water mixtures (indicated by ◈) are substantially lower than for the pure liquids. The upper solid curves which interconnect the wetting properties for water and methylene iodide provide calculated values of $\alpha_1 = 6.04$, $\beta_1 = 0.14$ (dyn/cm)$^{1/2}$ for the elastomer phase 1 and $\alpha_3 = 6.54$, $\beta_3 = 1.83$ (dyn/cm)$^{1/2}$ for the polyester phase 3. The dashed curves of Figure 7 which define the trend of wettability for the ethanol–water series of liquids provide calculated values of $\alpha_1 = 3.10$ and $\beta_1 = 2.05$ (dyn/cm)$^{1/2}$ for phase 1 and $\alpha_3 = 3.75$ and $\beta_3 = 3.64$ (dyn/cm)$^{1/2}$ for phase 3. The solid and dashed curves of Figure 7 would appear to define two independent types of adsorption interaction.

TABLE V
Surface Tension Properties of Hydroxyl Containing Liquids[a]

	γ_{Lv}, dyn/cm	γ_{Lv}^p, dyn/cm	β_L, $(\text{dyn/cm})^{1/2}$
Pure Liquid			
Water	72.2	50.1	7.08
Glycerol	63.4	31.6	5.62
Ethylene glycol	48.3	19.7	4.44
Polyglycol E-200	43.5	14.2	3.77
Polyglycol 15-200	36.6	8.3	2.88
Polyglycol 1200	31.3	7.2	2.68
X-Ethoxyethanol	28.6	5.0	2.24
Water–Ethanol Mixtures (vol-% H_2O)			
90	51.3	31.3	5.60
70	36.1	17.6	4.20
50	30.0	12.3	3.51
40	28.0	10.4	3.23
30	27.2	9.7	3.11
20	25.6	8.3	2.88
10	24.0	6.8	2.61
$\simeq 0$	22.7	5.4	2.32

[a] γ_{Lv} and γ_{Lv}^p data from Dann.[33]

A partial explanation for the deviation of the ethanol–water wettability data from the trends shown by pure hydroxy-containing liquids may be indicated by the data of Table V. The values of γ_{Lv} and γ_{Lv}^p for seven pure hydroxy liquids (including water) and eight ethanol–water mixtures as reported by Dann[33] are summarized in this listing and the associated β_L values tabulated. The results of evaluating these data for correlations between $\gamma_{Lv} = f(\gamma_{Lv}^p)$ and $\gamma_{Lv} = f(\beta_L)$ are shown in the curves of Figure 8. At equivalent values of γ_{Lv}, the ethanol–water series display higher values of γ_{Lv}^p which follow the relation

$$\gamma_{Lv}^p \simeq 0.89\ (\gamma_{Lv} - 16). \tag{24}$$

Alternatively, the pure hydroxy liquids display lower values of γ_{Lv}^p which appear to follow a linear function:

$$\beta_L = (\gamma_{Lv}^p)^{1/2} \simeq 0.93\ (\gamma_{Lv} - 8.0). \tag{25}$$

In the ethanol–water mixtures, the additional degrees of orientation and associative freedom for the hydroxy groups is evidently expressed in the higher γ_{Lv}^p values shown by the upper curve of Figure 8. Since the solid surfaces, as indicated by small β_1 and β_3 values to pure liquids, are only slightly polar, the ethanol–water liquids do not interact as efficiently as would be expected based on the given α_L and β_L values for these liquid mixtures. The following analysis will assume that the solid surface prop-

TABLE VI

Analysis of Phase 2 Immersion Effects on the Measured Work of Peeling W_c for a Bond with Interface Coefficients $H = 6.29$, $K = 0.99$, $R_4 = 0.88$ (dyn/cm)$^{1/2}$ [a]

Immersion phase 2	γ_{2v}, dyn/cm	α_2, (dyn/cm)$^{1/2}$	β_2, (dyn/cm)$^{1/2}$	S_2, dyn/cm	$\gamma_c^{1/2}$, (dyn/cm)$^{1/2}$	R, (dyn/cm)$^{1/2}$	W, dyn/cm
Vapor							
Air	0.0	0.0	0.0	−79.5	6.31	6.37	50000
Pure Liquids							
Water	72.8	4.67	7.14	−79.3	6.30	6.36	50000
Glycerol	63.4	5.83	5.48	−39.2	4.43	4.51	72500
Formamide	58.2	5.68	5.10	−33.0	4.06	4.15	38000
Ethylele glycol	47.7	5.41	4.36	−22.7	3.37	3.48	38000
Butanol	24.7	4.65	1.75	−6.0	1.58	1.78	19000
Ethanol	22.7	4.12	2.32	−11.4	2.39	2.55	22500
Liquid Mixtures (vol-%)							
90 H_2O/10 Ethanol	51.3	4.46	5.60	−47.6	4.88	4.96	38000
50 H_2O/50 Methanol	35.0	5.15	2.90	−8.3	2.08	2.23	26000

[a] Measured values of W at peel rate $r = 1$ cm/sec and 23°C from Gent and Schultz.[32]

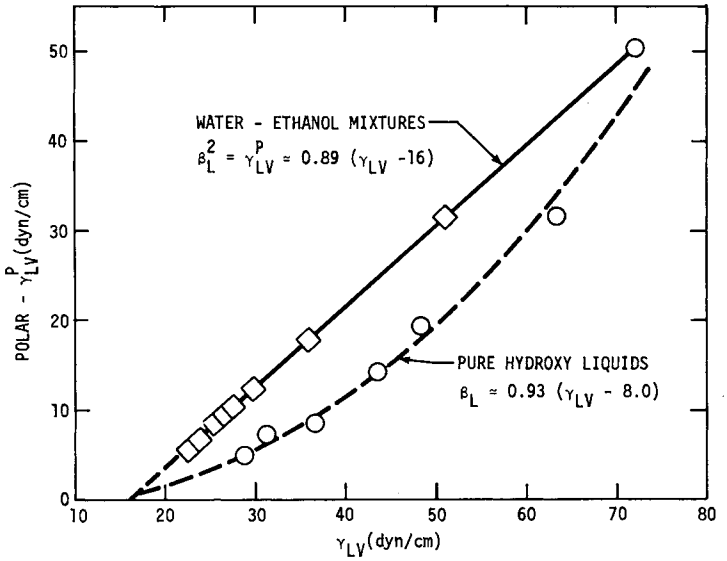

Fig. 8. Comparison of polar component γ_{Lv}^p of liquid surface tension γ_{Lv} for water–ethanol mixtures and pure hydroxy liquids.

erties of phase 1 and phase 3 are more accurately described by the upper solid curves of Figure 7.

Over the rate range $\dot{c} = dc/dt = 0.10$ to 1.0 cm/sec, the study of Gent and Schultz showed that the rate dependence of peel work W was defined by a constant $(d \ln W/d \ln \dot{c}) = 0.42$ for the various conditions of air and liquid immersion examined at 23°C. The measured values of $W = P/b$ at

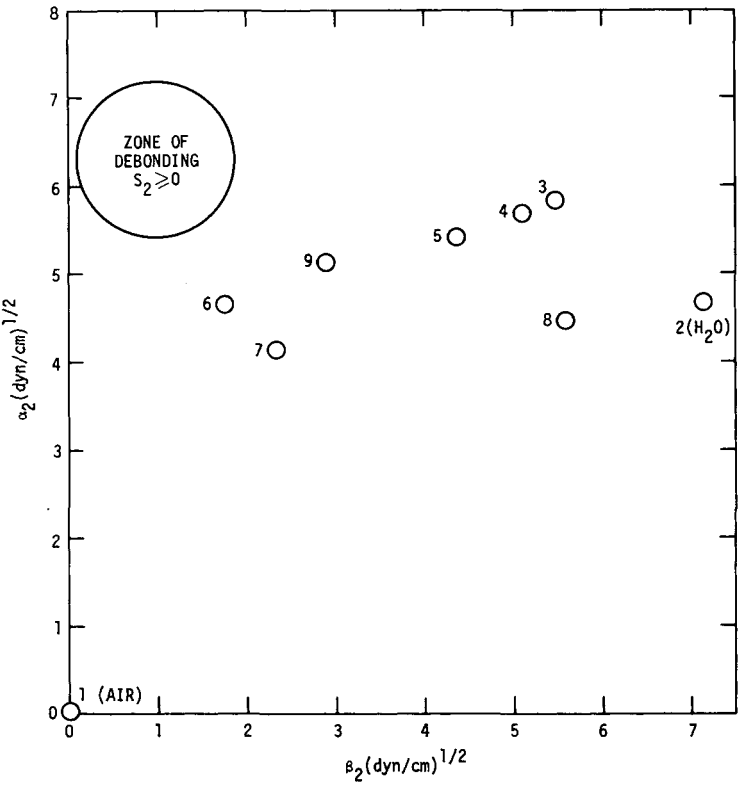

Fig. 9. Calculated zone of debonding, where $S_2 \geq 0$, for an elastomer–polyester interface relative to the α_2,β_2 surface properties of the immersion phase (2).

$\dot{c} = 1$ cm/sec are tabulated in the last column of Table VI and are seen to range from $W = 19000$ to 72500 dyn/cm, depending upon the condition of immersion.

Three types of phase 2 immersion are classified in Table VI as vapor phase, pure liquid and water–alcohol mixtures. The surface tension properties of all liquids, except butanol and 50 H_2O/50 methanol, are known. The values of α_2 and β_2 for these two liquids are estimated by eq. (25). By applying the α_1,β_1 and α_3,β_3 values, shown for pure liquid interactions in Table IV, the calculation of coefficients described by eq. (18) defines values of $H = 6.29$, $K = 0.99$, and $R_0 = 0.88$ (dyn/cm)$^{1/2}$. The graphic representation of these interface properties for the elastomer/polyester interface are shown as the circular region defined by $S_2 \geq 0$ in Figure 9. The surface properties of the ten immersion phases are represented as α_2,β_2 points on this reduced free-energy diagram. Since none of these values penetrates the $S_2 \geq 0$ region, we would predict $\gamma_c \geq 0$ and no spontaneous debonding. The middle columns of Table VI provide the calculated values of S_2, $\gamma_c^{1/2}$, and R as defined by eq. (18).

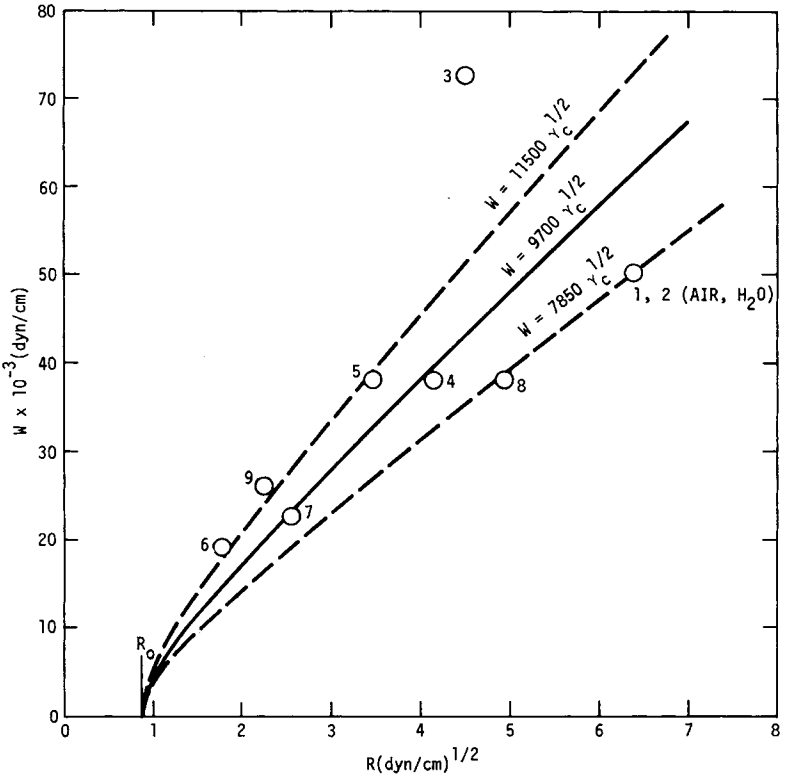

Fig. 10. Correlation between measured fracture energy W in peeling to calculated functions of $\gamma_c^{1/2}$.

The high magnitudes of the measured fracture energy $W = P/b$ reported in Table VI indicate $W_p \gg \gamma_c$ in eq. (21), so that the reversible fracture energy is an essentially negligible additive part of the total peel work W. Figure 10 plots the peeling work W values versus R values from the data reported in Table VI. This illustration shows that all immersion phases except glycerine can be defined by the function

$$W \simeq W_p = K \cdot \gamma_c^{1/2} \tag{26}$$

where the factor $K = 9700(\text{dyn/cm})^{1/2} \pm 20\%$. This experimental correlation appears to suggest an important new point not recognized by the Orowan fracture criteria of eq. (3). Evidently, there exists a functional interdependence between γ_c and W_p. In order words, $W_p = f(\gamma_c)$ and these two terms are highly interdependent for the case examined here.

Several significant points are illustrated by the analysis depicted graphically in Figures 9 and 10. Both illustrations predict that air and water should be equivalent as immersion media, and this result is confirmed in the experimental data. The theory explains this important result on the basis

that the radius R from the center of the $S_2 \geqslant 0$ zone of Figure 9 is equivalent for both air and water even though their surface properties appear at extreme positions on the α_2-versus-β_2 diagram. This result points out the importance of locating the $S_2 \geqslant 0$ zone of debonding by proper adjust of the interface properties $H = (\alpha_1 + \alpha_3)/2$ and $K = (\beta_1 + \beta_3)/2$. In other words, the interacting surface properties of phase 1 and phase 3 play a crucial role in determining environmental sensitivity and the magnitude of fracture toughness $W \approx W_p \approx K\gamma_c^{1/2}$.

The range of $K = 9700(\text{dyn/cm})^{1/2} \pm 20\%$ is not unexpected when one considers that this factor contains variability in both the measured values of peel work W and the calculations which define γ_c in eq. (25). The exceptional response of glycerol as an immersion media is not accounted for by this analysis. The suggestion of Gent and Schultz[32] that the high viscosity of glycerol may introduce a hydrodynamic contribution to W_p has merit. The glycerol viscosity effect, if dominant, would be expected to shift the rate dependence of peel work ($d \ln W/d \ln \dot{c}$) from its value in air immersion, but evidently the value ($d \ln W/d \ln \dot{c}$) = 0.42 applies for both media for the rate range $r = 0.10$ to 1.0 cm/sec.

SUMMARY AND CONCLUSIONS

This discussion develops a modified form for the fracture mechanics (F-M) fracture energy criteria in which the fracture surface energy γ_c is redefined in terms of current surface energetics (S-E) arguments. The resulting relations are employed to successfully analyze the effects of varied vapor and liquid phase immersion upon the energy requirements for interfacial crack propagation. The analysis shows that for any regular interface between solid phases 1 and 3, where $\alpha_1 \neq \alpha_3$ and $\beta_1 \neq \beta_3$, there exists a potential zone of spontaneous environmental debonding, even when the external stress $\sigma = 0$. This zone is defined by conditions $S_2 \geqslant 0$ or $R \leqslant R_0$ in eq. (18) or eq. (19).

Outside this zone of spontaneous debonding, where $S_2 \leqslant 0$ and $R > R_0$, the fracture energy is predicted to vary with the distance

$$R = [(\alpha_2 - H)^2 + (\beta_2 - K)^2]^{1/2}$$

independent of the balance of the values of α_2 and β_2 which describe the surface properties of the immersion phase. This prediction is substantially confirmed for the case of peeling in air, water, or other pure and mixed liquids.

Several important practical outcomes from this analysis are: (1) a method of characterizing surfaces and interfaces so as to minimize or maximize strength sensitivity to selected environments is defined; (2) a means is provided by which the reversible part γ_c of the total fracture energy can be analyzed independently and adjusted in order to study the functional relation $W_p = f(\gamma_c)$, where W_p is the irreversible plastic work of fracture

surface formation; (3) recognition from one analysis of experimental data that $W_p \propto \gamma_c^{1/2}$ for the case where $W_p >>> \gamma_c$.

The model developed for this discussion is specifically addressed to failure criteria at adsorption interfaces. The general analysis of interfacial bonding from which eq. (7) is taken also describes the thermodynamic and kinetic criteria for interdiffusion bonding in which case primary valence structure extends through the interface.[5,6]

The author wishes to thank Dr. C. L. Ho for helpful discussions. This work was supported in part by the North American Rockwell IR&D Interdivisional Technology Program under the sponsorship of the Composite Technical Panel.

References

1. A. A. Griffith, *Phil. Trans. Roy. Soc.* (London), **A221**, 163 (1921).
2. A. A. Griffith, *Proc. 2nd Int. Congr. Appl. Math., Delft*, 1924, p. 54.
3. G. R. Irwin, in *Structural Mechanics*, Pergamon Press, New York, 1960, pp. 557–594.
4. G. R. Irwin, in *Treatise on Adhesion and Cohesion*, R. L. Patrick, Ed., Dekker, New York, 1967, pp. 233–267.
5. D. H. Kaelble, *Physical Chemistry of Adhesion*, Wiley, New York, 1971.
6. D. K. Kaelble, *Proc. 23rd Int. Cong. on Pure and Applied Chem.*, Vol. 8, Butterworths, London, 1971, pp. 265–302.
7. C. E. Inglis, *Trans. Inst. Naval Arch.*, **60**, 219 (1913).
8. E. Orowan, *Fatigue and Fracture in Metals* (MIT Symposium, June, 1950) Wiley, New York, 1950.
9. W. A. Zisman, in *Adhesion and Cohesion*, P. Weiss, Ed., Elsevier, Amsterdam, 1962, p. 176.
10. J. P. Berry and A. M. Bueche, *ibid.*, p. 18.
11. E. P. Ripling, S. Mostovoy, and R. L. Patrick, *Mater. Res. Std.*, **4**, 129 (1964).
12. S. Mostovoy and E. J. Ripling, *J. Appl. Polym. Sci.*, **10**, 1351 (1966).
13. R. L. Patrick, J. A. Brown, L. E. Verhoeven, E. J. Ripling, and S. Mostovoy, *J. Adhesion*, **1**, 136 (1969).
14. E. J. Ripling, S. Mostovoy, and H. T. Corten, *J. Adhesion*, **3**, 107 (1971).
15. S. Mostovoy, E. J. Ripling, and C. F. Bersch, *ibid.*, p. 125.
16. E. J. Ripling, S. Mostovoy, and C. Bersch, *ibid.*, p. 145.
17. R. L. Patrick, W. G. Gehman, L. Dunbar, and J. A. Brown, *ibid.*, p. 165.
18. M. L. Williams, *Proc. 5th U.S. Congr. Appl. Mech.*, 451 (1966).
19. M. L. Williams, *J. Appl. Polym. Sci.*, **13**, 29 (1969); *ibid.*, **14**, 1121 (1970).
20. W. B. Jones and M. L. Williams, *The Measurement of Adhesive Energy in Fracture Investigations*, UTEC DO 68-019 University of Utah, February, 1968.
21. J. D. Burton, W. B. Jones, and M. L. Williams, *Trans. Soc. Rheol.*, **15**, 39 (1971).
22. M. L. Williams, Proc. 9th Conf. on Adhesion and Adhesives, City University London, April 1971 (UTEC DO 71-068 University of Utah).
23. H. Dannenberg, *J. Appl. Polym. Sci.*, **5**, 125 (1961).
24. F. M. Fowkes, in *Treatise on Adhesion and Adhesives*, R. L. Patrick, Ed. Dekker, New York, 1967, Chap. 9.
25. R. J. Good, *ibid.*, Chap. 2.
26. K. C. Uy and R. Chang, in *Dental Restorative Materials*, Vol. 2, PHS Publication 1494, Government Printing Office, Washington, D.C., 1966, Chap. 3.
27. D. Owens and R. Wendt, *J. Appl. Polym. Sci.*, **13**, 1741 (1969).
28. R. K. S. Chan, *J. Colloid Interfac. Sci.*, **32**, 492, 499 (1970).
29. F. H. Kaelble and K. C. Uy, *J. Adhesion*, **2**, 50 (1970).

30. D. H. Kaelble, *J. Adhesion*, **2**, 66 (1970).
31. D. K. Owens, *J. Appl. Polym. Sci.*, **14**, 1725 (1970).
32. A. N. Gent and J. Schultz, *J. Adhesion*, **3**, 281 (1972).
33. J. R. Dann, *J. Colloid Interfac. Sci.*, **32**, 302 (1970).

Received October 3, 1973